RSC Advances

PAPER

View Article Online
View Journal | View Issue

Published on 14 November 2014. Downloaded by National Chiao Tung University on 21/07/2015 10:48:35.

Cite this: *RSC Adv.*, 2014, **4**, 64525

A quenching method for the preparation of metal oxide–polythiophene composites having fiber structures

Fang-Hsien Lu,[a] Mohamed-Gamal Mohamed,[b] Tzeng-Feng Liu,[a] Chuen-Guang Chao,*[a] Lizong Dai[c] and Shiao-Wei Kuo*[b]

Received 12th November 2014
Accepted 13th November 2014

DOI: 10.1039/c4ra14371j

www.rsc.org/advances

In this study we developed a simple quenching method to fabricate metal oxide (CuO, ZnO, TiO_2, $Fe(OH)_3$)–polythiophene (PT) composites. By varying the metal oxide, PT, and rate of crystallization, we could control the fiber morphology in these composites. Four-probe-station analyses revealed that the conductivities of these metal oxide–PT composites ranged from 10^{-5} to 10^{-3} S cm^{-1}, higher than that of any species of metal oxide alone (from 10^{-10} to 10^{-7} S cm^{-1}), because the fiber morphology behaved as an exceptional transmission factor for electrons. Moreover, these metal oxide–PT composites exhibited the characteristics of colloids, as well as high viscosity, suggesting that they could also be applied as coatings on silicon and glass substrates, and could provide the opportunity to form useful materials for large-scale gas sensors due to good flexibility and porosity. UV-vis spectroscopic analyses revealed variations in the energy level (>3.37 eV for ZnO) and confirmed the mechanism of the morphology change of the composite.

Introduction

Many fabrication methods, including the vapor–liquid–solid (VLS) method, metal–organic chemical vapor deposition, physical vapor deposition (PVD), and microwave hydrothermal methods, can be employed to produce thin materials for application in nanotechnology. For example, ZnO nanowire[1] and nanorod arrays are often prepared using the VLS method, even through this method is restricted by the need for high temperatures. Similarly, ZnO nanosheets and branch structures can be obtained through the PVD method, which also requires stringent conditions (*e.g.*, high vacuum).[2] Likewise, hydrothermal[3–6] and laser ablation[7–10] methods can be performed only under severe conditions.

Accordingly, industrial and academic researchers are seeking new facile methods for the preparation of nanomaterials at relatively low costs. Fabrication involving many kinds of nanostructures, including nanodendrites,[11–13] can be accomplished inexpensively using, for example, chemical solutions,[14–16] solvothermal reactions,[17,18] and water baths. In the present study, we developed a new technique, a so-called "quenching method," for manufacturing metal oxide/polymer fibers. This quenching method involves setting the precipitation properties of the metallic and ceramic materials at low temperatures and controlling the nucleation rate[19–21] and the growth orientation[22–24] of the nanostructures. Noble metal nanoparticles of uniform size can be fabricated through a drastic variation of temperature in a microwave hydrothermal procedure as the result of a rapid rate of nucleation among the metal atoms. Moreover, a slow rate of crystallization can occur at low temperatures, leading to the formation of rod structures with a fixed growth orientation.

Among the various nanostructures, fiber structures are interesting research materials because they possess large aspect ratios, resulting in large specific surface areas, high activities, and good growth orientation. The conditions for controlled growth of fiber structures can, however, involve exposure to harsh environments. A quenching method could, therefore, become a profitable means of fabricating fiber structures. Because a high affinity exists between metal cations and thioethers, which are the subunits of polythiophene (PT) structures, such polymers can bind to metal cations and affect their stacking when fabricating metallic compound–polymer fiber structures. We suspected that such fiber structures might improve the efficiency of photoelectric devices. Hence, in the present study we used this quenching method to manufacture composite materials exhibiting high conductivity and high elasticity for improving capacitance and applications in the electrodes of solar cells and gas sensors. Moreover, the fiber

[a]*Department of Materials Science and Engineering, National Chiao Tung University, Hsinchu 300, Taiwan. E-mail: cgchao@gmail.com*

[b]*Department of Materials and Optoelectronic Science, Center for Functional Polymers and Supramolecular Materials, National Sun Yat-Sen University, Kaohsiung, 804, Taiwan. E-mail: kuosw@faculty.nsysu.edu.tw*

[c]*Department of Material Science and Engineering, Fujian Provincial Key Laboratory of Fire Retardant Materials, College of Materials, Xiamen University, Xiamen, Fujian, 361005, China*

Published on 14 November 2014. Downloaded by National Chiao Tung University on 21/07/2015 10:48:35.

structure, including good flexibility, tensile strength, and porosity, can improve the adsorption ability and detection limit of large-scale gas sensors. Even the preparation of the transporting layers of solar cells are simplified by using metallic compound–polymer composites with high viscosity and coating properties.

Experimental

Materials

$FeCl_3$ (assay: ≥99.99% trace metal basis; M_p: 304 °C), $CuCl_2$ (assay: ≥99.995% trace metal basis; M_p: 620 °C; $d = 3.38$ g cm^{-3} at 25 °C), $ZnCl_2$ (assay: ≥99.995% trace metal basis; M_p: 293 °C; B_p: 732 °C per 1 atm), $TiCl_3$ (assay: ≥99.995% trace metal basis; M_p: 440 °C), thiophene (C_4H_4S; assay: ≥99%; B_p: 84 °C), poly(vinyl alcohol) ($(C_2H_4O)_n$; molecular weight: 89 000–98 000 g mol^{-1}), and NaOH (assay: ≥98%; total impurities: ≤1.0% Na_2CO_3) were purchased from Sigma-Aldrich. Ethylene glycol ($C_2H_4(OH)_2$; M_p: −13 °C; B_p: 194 °C; $d = 1.11$ g cm^{-3}) was obtained from J. T. Baker.

Metal oxide–polymer complexes

A fixed quantity of a metal chloride powder was dissolved in ethylene glycol to prepare a solution having a concentration of 32 000 ppm. This solution was mixed with 3 wt% poly(vinyl alcohol) and stirred at 70 °C for 1 h. Thiophene [6.4 g (0.076 mol), 9.6 g (0.114 mol), or 12.8 g (0.152 mol)] was injected *via* syringe. The mixture was stirred continuously at 70 °C for 1 h before cooling rapidly to −40 °C in a liquid nitrogen mixed system. 3 M NaOH was added slowly to the mixture. A metal hydroxide—brown $Fe(OH)_3$, blue $Cu(OH)_2$, or white $Zn(OH)_2$—precipitated rapidly. The mixtures were maintained at −40 °C for a period of time to completely convert the metal chloride to the metal hydroxide. Subsequently, the whole solution, including the precipitate, was stirred at 70 °C for 1 h and then quenched rapidly once again. Finally, the precipitate, corresponding to the product, was washed several times through centrifuging and filtering and was then dried at 65 °C in a precise oven.

Characterization

The structures and compositions of the products were identified through X-ray diffraction (XRD) using a Bruker D8 DISCOVER apparatus; the wavelength (λ) of the incident beam (1.5412 Å) was set using a rotating Cu target. The morphologies and shapes of the nanomaterials were observed through field emission scanning electron microscopy (FE-SEM), using a JSM-7000F microscope (JEOL, Japan), and optical microscopy (OM), using an Olympus BX51-P microscope. The energy levels of the metal oxide–polymer composites were measured using UV-vis-NIR spectrophotometry (Hitachi U-4100). Electrical properties, including conductivity, were measured using four-probe-station analysis (Hewlett–Packard). Samples for conductivity analysis were prepared in tablet form for comparison with the bulk pure metallic composite.

Results and discussion

Compositions of the products

Fig. 1 displays the structures and compositions of the products fabricated using the metal chloride–poly(vinyl alcohol)–thiophene (MPT) systems. The characteristic peak of PT appeared distinctly at a 2θ value of 2.3–6.3°.[25–27] The presence of ZnO, CuO, and TiO_2 was confirmed by their JCPDS signals; however, an amorphous phase occurred for $Fe(OH)_3$, because of its self-crystalline characteristics. Furthermore, we observed the characteristic crystalline peak of poly(vinyl alcohol) at a 2θ value of 17–20° in the XRD patterns; the intensity of this peak was weak, however, because poly(vinyl alcohol) functioned as a water-soluble surfactant in our reaction media and was mostly rinsed out from the products. The mechanisms of formation of the metallic compounds presumably occurred as follows:

(a) Formation of CuO

$$CuCl_2 + 2NaOH \rightarrow Cu(OH)_2 + 2NaCl$$

$$Cu(OH)_2 \rightarrow CuO + H_2O \text{ (heating at 70 °C)}$$

(b) Formation of ZnO

$$ZnCl_2 + 2NaOH \rightarrow Zn(OH)_2 + 2NaCl$$

$$Zn(OH)_2 \rightarrow ZnO + H_2O \text{ (heating at 70 °C)}$$

(c) Formation of TiO_2

$$2TiCl_3 \rightarrow TiCl_2 + TiCl_4 \text{ (in solution)}$$

$$TiCl_4 + 2H_2O \rightarrow TiO_2 + 4HCl$$

$$TiO_2 + 4HCl + 2NaOH \rightarrow TiO_2 + 4H_2O + 4NaCl$$

(d) Formation of $Fe(OH)_3$

$$FeCl_3 + 3NaOH \rightarrow Fe(OH)_3 + 3NaCl$$

$$2Fe(OH)_3 \rightarrow Fe_2O_3 + 3H_2O \text{ (requires heating at 300 °C)}$$

The structures of the products were transformed when adding thiophene, as shown in Fig. 1(a) and (b). Fig. 1(b) presents the structures fabricated using the metal chloride–poly(vinyl alcohol)–thiophene (0.152 mol) systems (MPT152). The intense signal for the crystallization of the metal oxide weakened in each spectrum, with the trend toward an amorphous structure being most remarkable for the $CuCl_2$–poly(vinyl alcohol)–thiophene (0.152 mole) system (CuPT152). Furthermore, in the ZnPT152 system, most of the strongest peaks were located at higher values of 2θ. These results indicate that the structures of the metal oxides changed from ordered [Fig. 1(a)] to disordered [Fig. 1(b)].

 This journal is © The Royal Society of Chemistry 2014

Published on 14 November 2014. Downloaded by National Chiao Tung University on 21/07/2015 10:48:35.

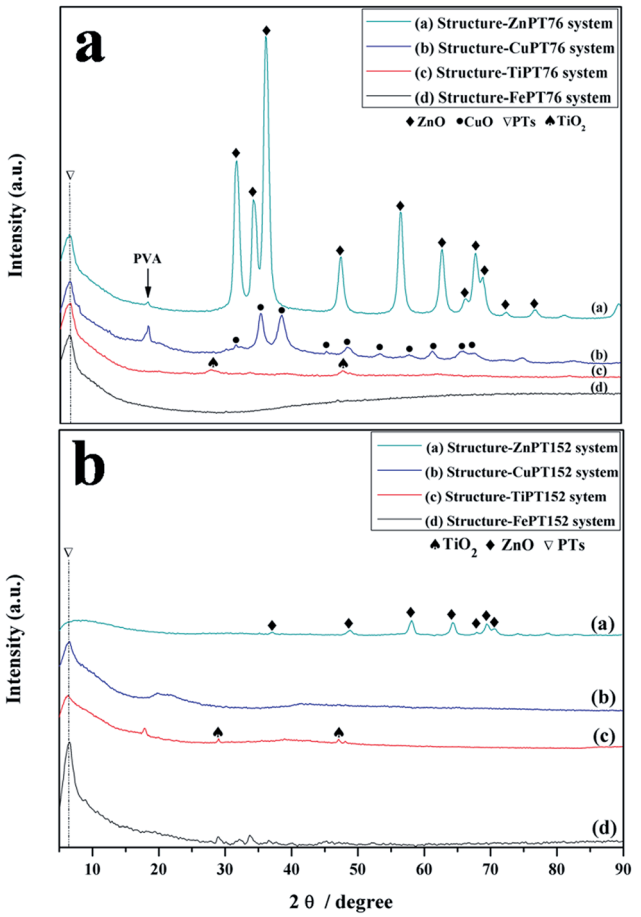

Fig. 1 XRD patterns of the products fabricated using the (a) MPT76 and (b) MPT152 systems.

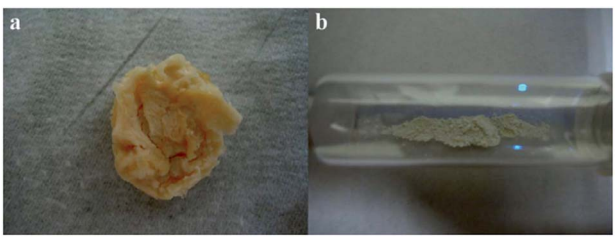

Fig. 2 Products fabricated using the ZnPT76 system when using the (a) quenching and (b) hydrothermal methods.

Fig. 3 shows the shapes of the metal oxide–polymer complexes fabricated using the MPT systems using the quenching method. The metal oxide–polymer complexes possessed the elastic properties of colloids before and after drying [Fig. 2(a)]. In contrast, the metal oxide–polymer complexes had powdery properties when fabricated using the hydrothermal method [Fig. 2(b)]. Fig. 3 and 4 display OM and SEM images, respectively, of the complexes fabricated using the metal chloride–poly(vinyl alcohol)–thiophene (0.114 mol) systems (MPT114). Each of these complexes possessed the morphology of irregular fibers; this morphology disappeared when we fabricated the complex from a metal chloride–poly(vinyl alcohol) system (Fig. 5). We suspect that the mechanism of fiber formation occurred as follows. In the MPT system, poly(vinyl alcohol) and ethylene glycol have similar solubility capabilities and can be regarded as surfactants. Polymerization of the thiophene monomers to form PT was mediated by $FeCl_3$ or $CuCl_2$ at low temperature. As mentioned above, these metal cations have an affinity for thioether units. Hence, the stacking in the metal oxide lattices was affected by the presence of the PT. After quenching, the low temperature decreased the rates of nucleation and growth. In other words, the lattice of the metal oxide could stack appropriately, with the PT units in contact with the sides of the metal oxide lattices. Fig. 6 illustrates the structure of a fiber, presenting the arrangement of the lattices of the metal oxide and the chains of PT. The hexagonal lattices represent the ZnO crystals; the growth orientation of the fiber structure of the ZnO–PT complex is indicated in the (101) plane, as determined by comparing the XRD data from this study with those in the JCPDS database.[28,29] In contrast, the PT chains formed irregular and disordered structures. Hence, the orientation of the metallic composite was not fixed efficiently. The low temperature was another factor that affected the formation of the rods from the metal oxide–polymer complexes. According to the following thermodynamic functions:

$$D^2 - D_0^2 = K_0 e^{-Q/RT}, \quad (1)$$

$$\log\left(D^2 - \frac{{D_0}^2}{t}\right) = -\left(\frac{Q}{2.3RT}\right) + \log K_0, \quad (2)$$

where D_0 is the initial grain size, D is the final grain size, K_0 is a constant, T is the absolute temperature and Q is the activation energy for boundary mobility, the driving force for metal oxide nanoparticles and the stacking rate would decrease gradually upon decreasing the temperature. These phenomena would cause the grain sizes of the metallic composites to increase. Thus, micrometer-scale rods would grow from these metallic composites.

OM (Fig. 7) revealed the existence and arrangement of the PT in the complexes. Fig. 8 and 9 present SEM images showing the morphologies of the complexes formed from the metal chloride–poly(vinyl alcohol)/thiophene (0.076 mol) systems (MPT76) and the MPT152 systems, respectively. For the MPT76 systems, we observed fiber morphologies for the complexes; transformation from fibers to a silk-like morphology occurred after increasing the amount of added thiophene to 0.152 mol. Further physical differences existed between these two systems. For instance, the silk-like morphology fabricated using the CuPT152 system exhibited fluorescence under polarized-light OM (Fig. 10), whereas the fiber morphology fabricated using the CuPT76 system exhibited little of this behavior. The fluorescence emission originated from the great amount of the conjugated polymer PT in the CuO–PT complex. Thus, the morphology and structure of the metal oxide–PT complex could be transformed by varying the content of thiophene in the reaction medium; these changes also affected the conductivity and absorption. Thus, when the signal in the XRD spectrum for the (100) plane at 2θ values of 2.3–6.3° became flat in the presence of the PT, the

Published on 14 November 2014. Downloaded by National Chiao Tung University on 21/07/2015 10:48:35.

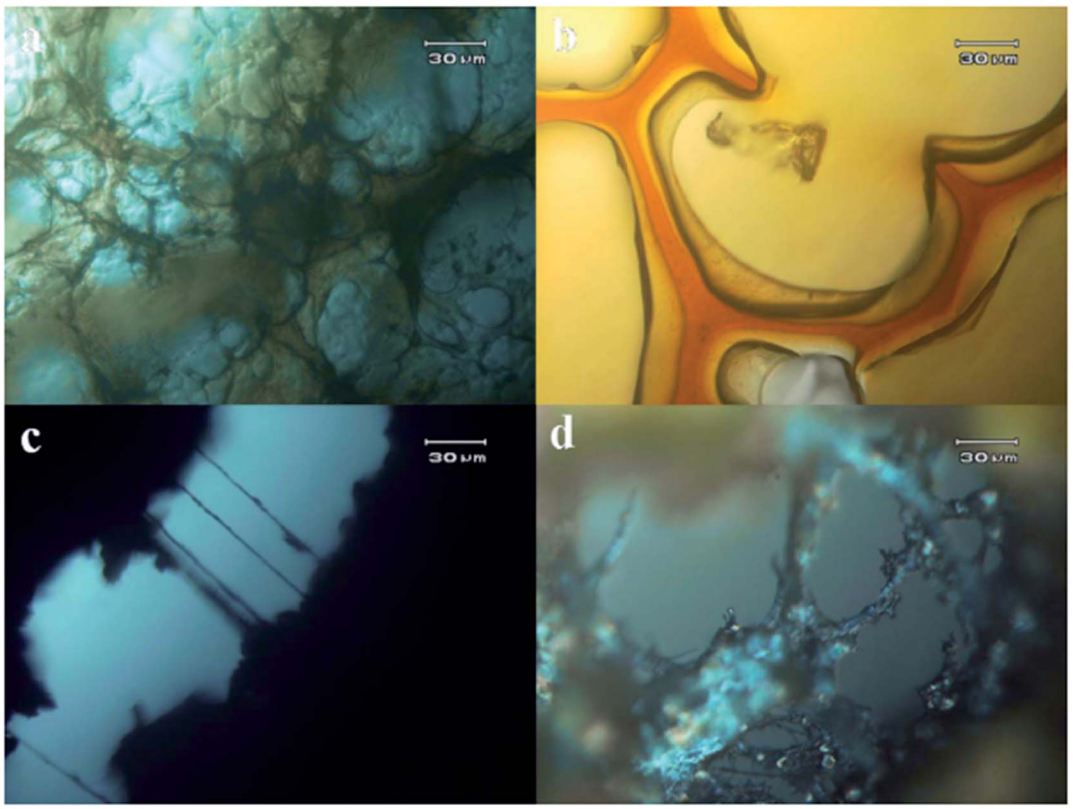

Fig. 3 OM images displaying the morphologies of the products fabricated using the MPT114 system: M = (a) Cu, (b) Fe, (c) Zn, and (d) Ti.

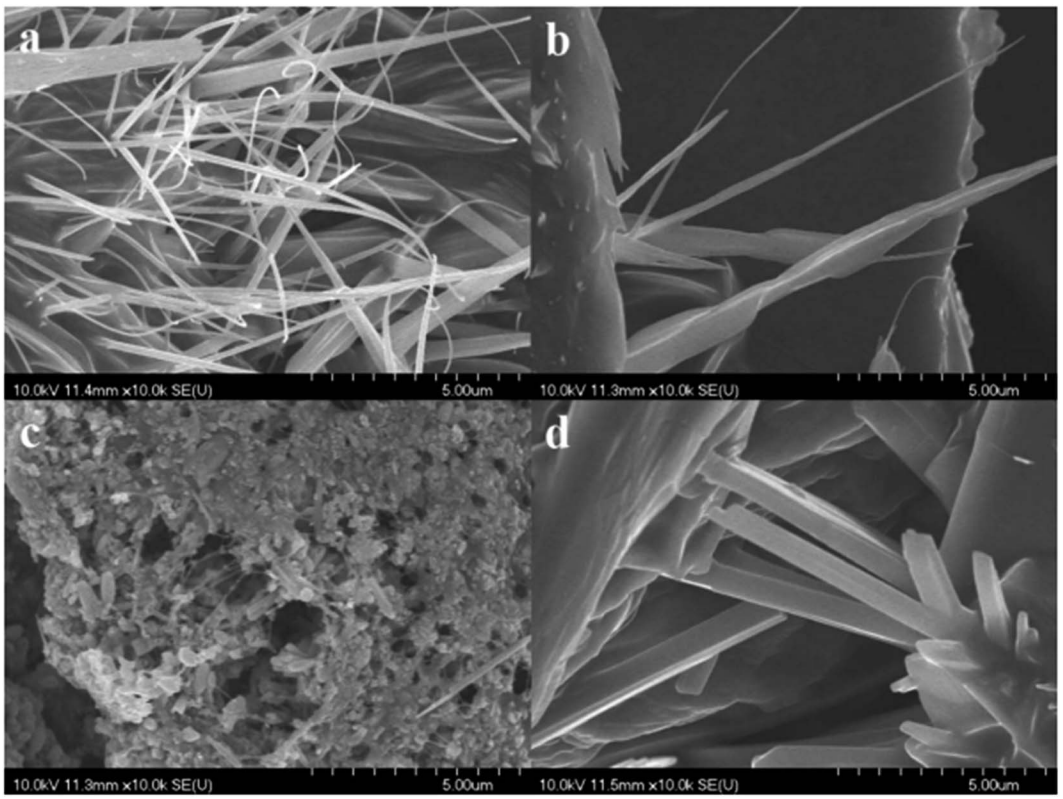

Fig. 4 SEM images displaying the morphologies of the products fabricated using the MPT114 system: M = (a) Cu, (b) Fe, (c) Zn, and (d) Ti.

This journal is © The Royal Society of Chemistry 2014

Published on 14 November 2014. Downloaded by National Chiao Tung University on 21/07/2015 10:48:35.

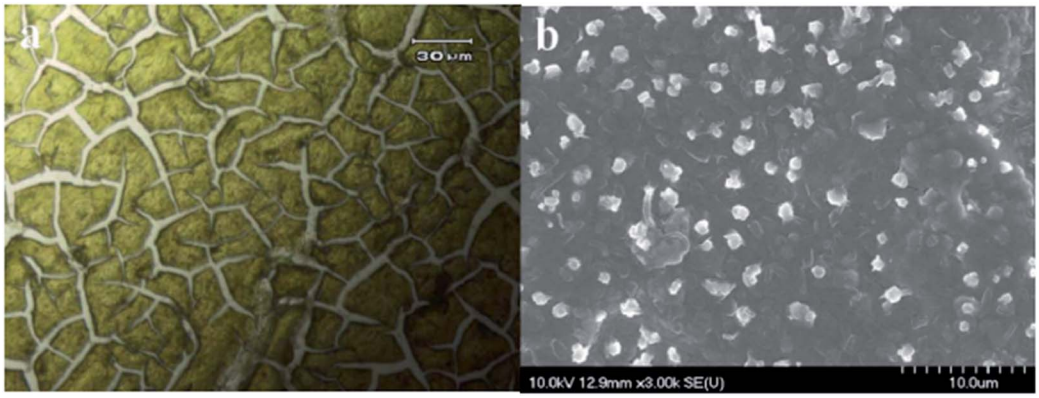

Fig. 5 (a) OM and (b) SEM images displaying the morphology of the product fabricated using the CuPT system using the hydrothermal method.

morphology of the complex became silk-like, due to the lower compatibility between the metallic composite and the PT. In other words, the structure of the complex was disrupted in the presence of a greater amount of PT. Hence, good stacking of the lattices of the metallic composites was not compatible with the PT chains. Table 1 summarizes the morphologies with different amounts of thiophene monomer and different metal precursors.

We also measured the critical bonding C–S–C,[30] C–S(O_2)–C, and S–metal species using XPS as shown in Fig. 11. From this figure, the C–S–C and C–S(O_2)–C species, respectively, were confirmed from the 161.5–163 eV and 164.5–167.5 eV regions. Moreover, the most important bonding, representing the S-metal chelation as S–Ti, could be found in the region of 160–161 eV, and this binding energy region is regularly used to identify the chelating interaction of thio-metals, such as thio-tungsten.[31]

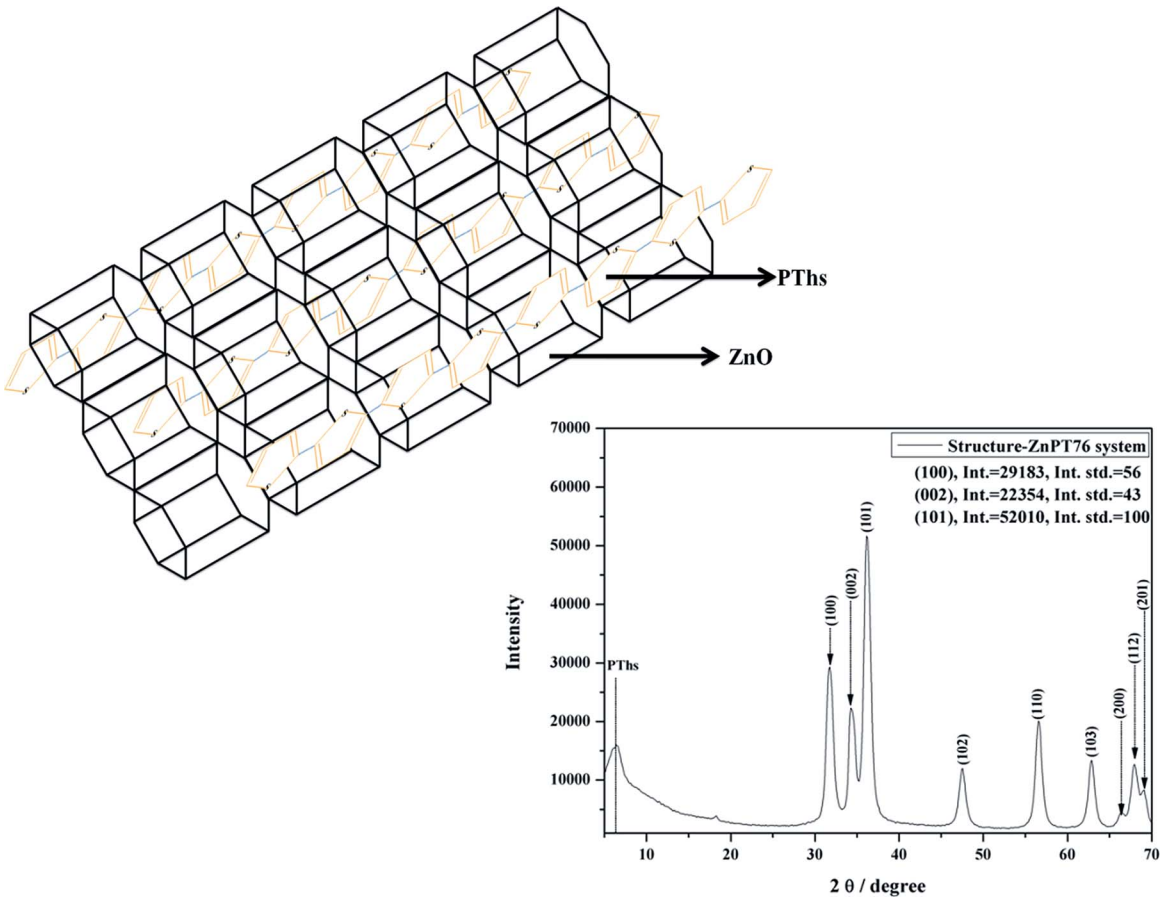

Fig. 6 Structures of the products fabricated using the ZnPT76 system (inset figure is X-ray diffraction pattern for ZnPT76 system).

Published on 14 November 2014. Downloaded by National Chiao Tung University on 21/07/2015 10:48:35.

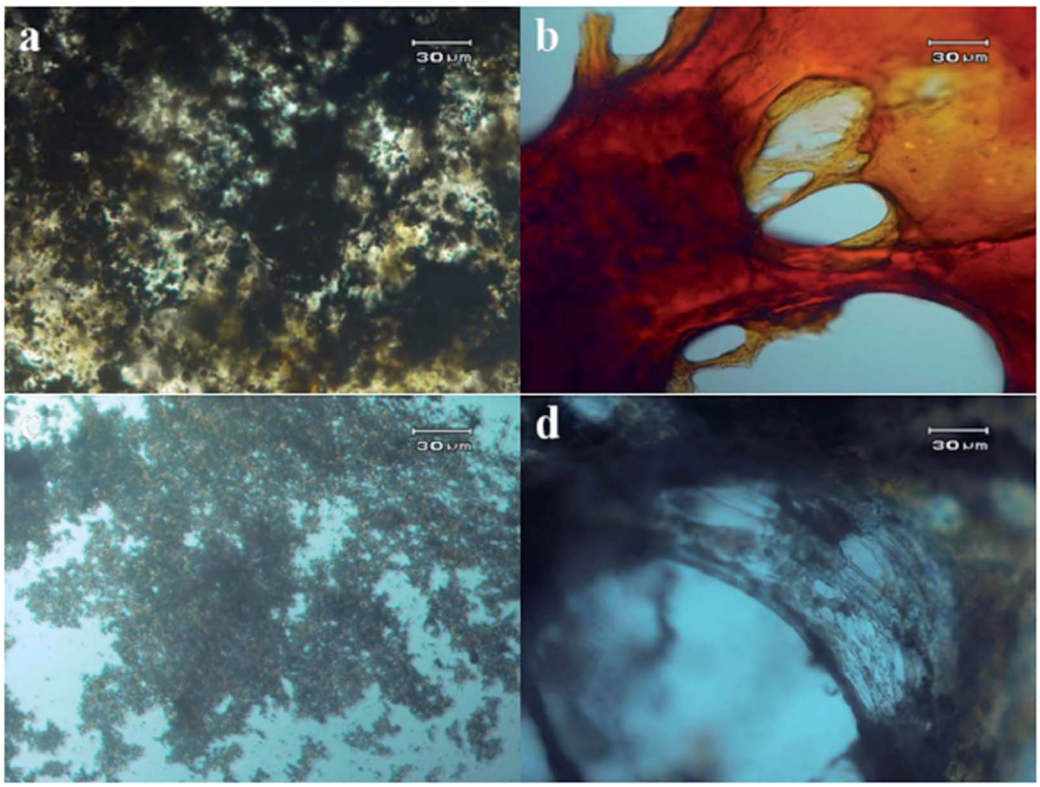

Fig. 7 OM images displaying the morphologies of the products fabricated using the MPT76 system: M = (a) Cu, (b) Fe, (c) Zn, and (d) Ti.

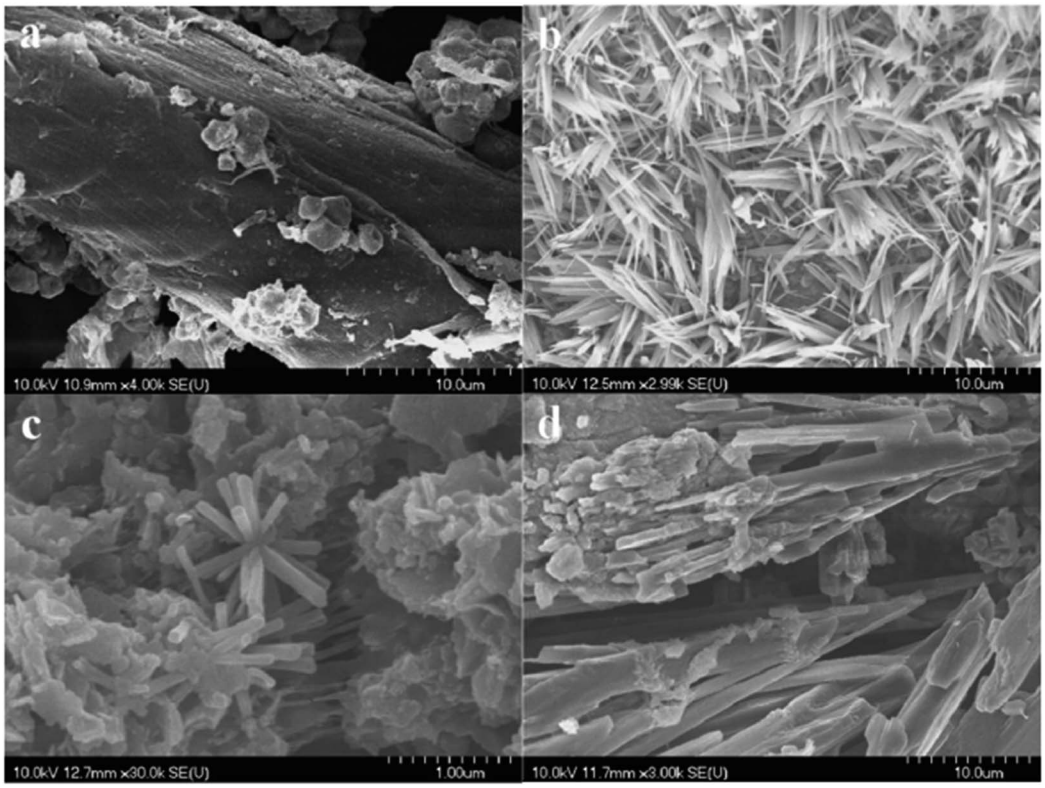

Fig. 8 SEM images displaying the morphologies of the products fabricated using the MPT76 system: M = (a) Cu, (b) Fe, (c) Zn, and (d) Ti.

This journal is © The Royal Society of Chemistry 2014

Published on 14 November 2014. Downloaded by National Chiao Tung University on 21/07/2015 10:48:35.

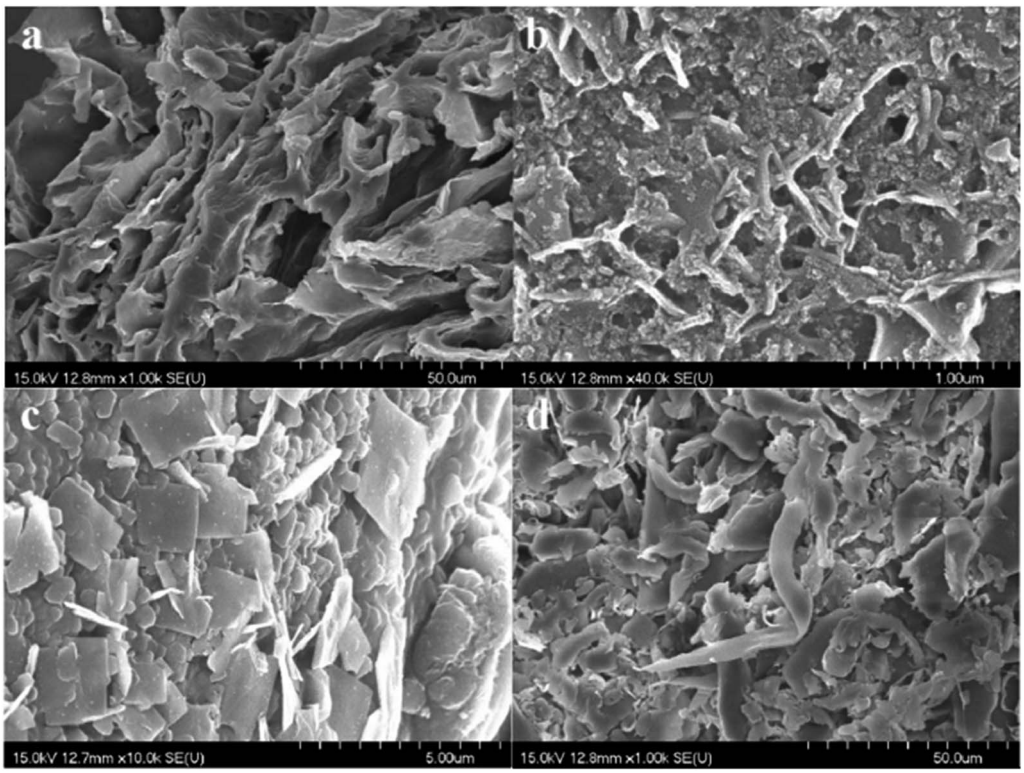

Fig. 9 SEM images displaying the morphologies of the products fabricated using the MPT152 system: M = (a) Cu, (b) Fe, (c) Zn, and (d) Ti.

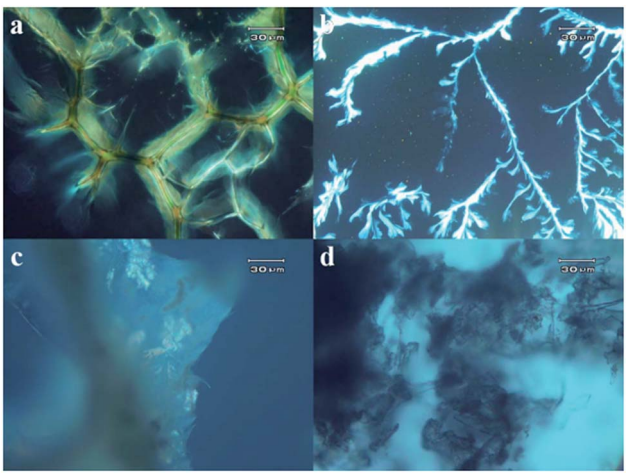

Fig. 10 OM images displaying the morphologies of the products fabricated using the MPT152 system: M = (a) Cu, (b) Fe, (c) Zn, and (d) Ti.

Table 1 Morphology change with different amounts of thiophene monomer and different metal precursors

Amount of thiophene monomer	Metal precursor	Morphology
0.076 mole	$CuCl_2$	Fiber
0.114 mole	$CuCl_2$	Fiber
0.152 mole	$CuCl_2$	Silk
0.076 mole	$FeCl_3$	Fiber
0.114 mole	$FeCl_3$	Fiber (needle)
0.152 mole	$FeCl_3$	Silk
0.076 mole	$ZnCl_2$	Rod
0.114 mole	$ZnCl_2$	Rod, fiber
0.152 mole	$ZnCl_2$	Silk
0.076 mole	$TiCl_3$	Rod
0.114 mole	$TiCl_3$	Rod, fiber
0.152 mole	$TiCl_3$	Silk

Conductivity of the complexes

Fig. 12 displays the conductivity curves of the metal oxide–PTs fabricated using the MPT systems. We observed a low conductivity (2.7×10^{-12} S cm^{-1}) for the p-type semiconductor CuO in the absence of PT. In contrast, the CuO–PT complex fabricated using the CuPT76 system exhibited a conductivity of 3.9×10^{-5} S cm^{-1}. Rutile TiO_2, which has a conductivity of 1×10^{-12} S cm^{-1}, is a familiar p-type semiconductor; we measured a conductivity of 1.4×10^{-4} S cm^{-1} for the TiO_2–PT complex fabricated using the TiPT76 system. Although metal oxides have high resistivity (*e.g.*, 1.8×10^6 Ω cm for ZnO), we observed an increased conductivity (to 5.5×10^{-6} S cm^{-1}) for the fiber morphology of the ZnO–PT complex fabricated using the ZnPT76 system. Furthermore, both the polymers and the metal hydroxides can be considered, in isolation, as insulating materials. For example, $Fe(OH)_3$ and PT possess conductivities of 1×10^{-9} and 1×10^{-6} S cm^{-1}, respectively. Although the conductivities of PTs are typically higher than those other conjugated polymers, they are much lower than that of our $Fe(OH)_3$–PTs complex.

Published on 14 November 2014. Downloaded by National Chiao Tung University on 21/07/2015 10:48:35.

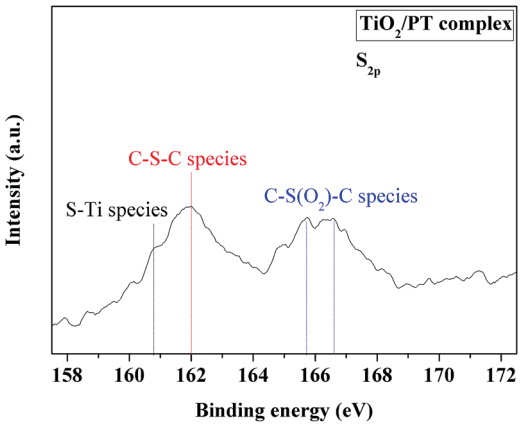

Fig. 11 The XPS results for the TiO_2–PT complex.

Thus, the fiber morphology decreased the resistivity significantly, primarily because the fiber morphology could supply electrons for transmission and excitation over a short distance. This corresponds to the fiber structure supplying a very conductive route for holes and electrons, where the electrons would waste little energy in intermolecular transfer; however, a greater loss of energy would occur in a discontinuous particle structure. Therefore, as in other work on electrospun materials, the polymeric fiber materials can promote the interlinking of the discrete metal particles to give good conduction properties. The conductivities of our metal composite–PT systems changed from high to low, however, upon increasing the amount of thiophene in the reaction mixtures—the result of changing the morphology in the metal composite–PT complex from fibers to silk-like structures. Accordingly, the electrons could not undergo efficient conduction. On the other hand, the mechanism of conduction for a semiconductor requires the generation of electron–hole pairs. Therefore, its conductivity is less than that of a metal because the electrons of the valence band require sufficient energy to transition into a conductive band. In this case, a disrupted metal structure would exist in the excessive PT system; this was polycrystalline and the increased number of grain-boundaries in the structure restricted the transmission of electrons. In comparison, in a single-crystalline metal oxide structure, the intermolecular movement of electrons is unrestricted. The disrupted metal oxide structure has been proven by XRD [Fig. 1(b)]. The literature states that highly regular PT structures can form when its polymerization is restricted at low temperatures. Good π–π stacking exists in such PT structures, resulting in good conductivity. Although the conductivities of our metallic composite–PT systems tended to be low after transformation of their morphologies from fiber to silk-like structures, the conductivities of these complexes remained in the range of 10^{-5} to 10^{-4} S cm^{-1} because they possessed firm structures with good transmission factors for electrons.

Photophysical properties of metallic composite–PT

Fig. 13(a)–(c) display the UV-vis absorption spectra of the metallic composite–PT complexes; the energy level of each complex was located in the range from 3.75 to 4.27 eV. The absorption of PT typically occurs in a wavelength range of 431–450 nm,[32] but this absorption disappears in a complex such as TiO_2–PT because of the occurrence of energy transfer. In other words, the electrons in the electronic band of the metallic

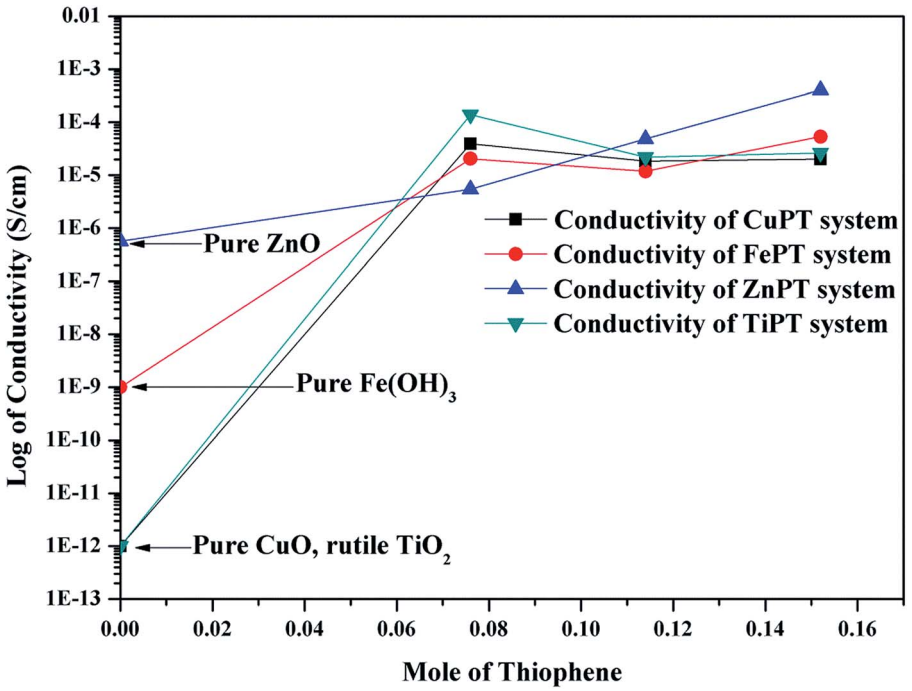

Fig. 12 Conductivity curves of the metallic composite–PT complexes fabricated using the MPT systems.

 This journal is © The Royal Society of Chemistry 2014

Published on 14 November 2014. Downloaded by National Chiao Tung University on 21/07/2015 10:48:35.

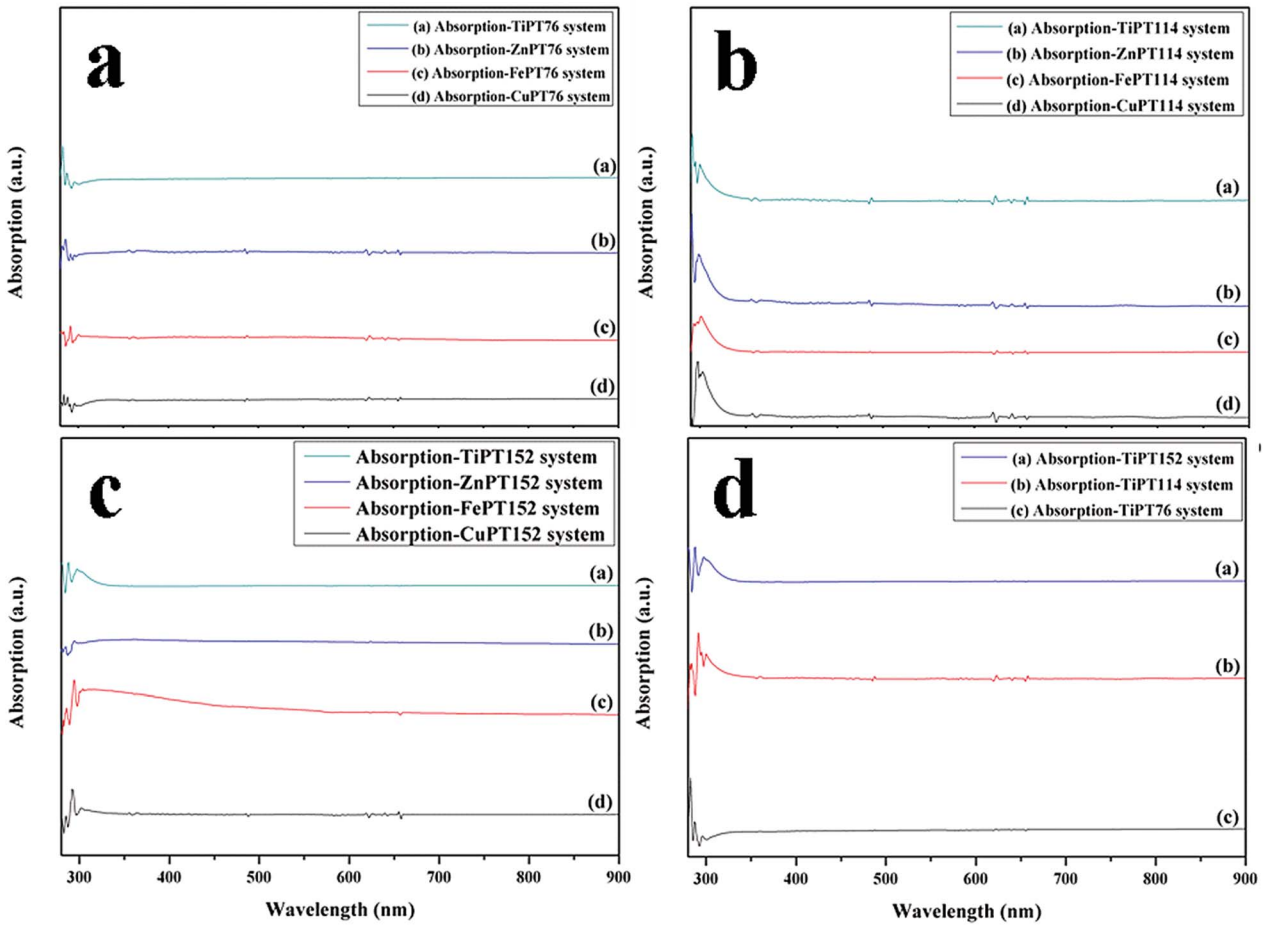

Fig. 13 Absorption spectra of the products fabricated using the (a) MPT76, (b) MPT114, (c) MPT152, and (d) TiPT systems.

composite can jump to the lowest unoccupied molecular orbital (LUMO) of PT after excitation under UV irradiation. On the other hand, the phenomenon in which an electron in the valence band of the metallic composite can transfer into the lowest unoccupied molecular orbital of the PT over a short distance will enhance the conductive properties of the complex. As a result, the energy levels of our complexes were greater than those of the metal oxide or PT alone, due to transitions in the morphologies and energy levels. For example, Fig. 13(d) presents the spectra of the TiO_2–PT complexes fabricated using the TiPT76, TiPT114, and TiPT152 systems. A blue-shift in the absorption wavelength occurred as the morphology transformed from silk-like to a fiber structure. The electrons transferred from the conductive band of the metallic composite to the LUMO of the PT after passing its valence band; hence, the electrons required more energy to overcome the energy levels.[33,34]

Conclusions

By applying a facile and novel technique, a quenching method, we have fabricated metallic composite–PT complexes exhibiting fiber morphologies and excellent conductivities. The high affinity between a metallic composite and PT affected the ratios of nucleation and growth, resulting in the complexes having a fiber morphology. These complexes exhibited conductivities, ranging from 10^{-5} to 10^{-3} S cm^{-1}, that were higher than those of the pure metallic composites or of PT because the fiber morphologies enhanced the conduction of electrons. In addition, the complexes possessed the properties of colloids, suggesting that they could be coated on most types of substrate, including glass; moreover, these complexes could be applied in large-scale gas sensors due to their flexibility and porosity, and could even simplify the preparation of transporting layers of solar cells.

Acknowledgements

We thank Professor Cheng Chien Lin and his group at the National Chiao Tung University for XRD analysis as well as the Ministry of Science and Technology, Republic of China, for financial support (MOST 100-2221-E-110-029-MY3 and MOST 102-2221-E-110-008-MY3). In addition, Prof. Dai would like to thank the National Natural Science Foundation of China (U1205113).

Published on 14 November 2014. Downloaded by National Chiao Tung University on 21/07/2015 10:48:35.

References

1 D. I. Suh, C. C. Byeon and C. L. Lee, *Appl. Surf. Sci.*, 2010, **257**, 1454–1456.
2 G. Jimenez-Cadena, E. Comini, M. Ferroni, A. Vomiero and G. Sberveglieri, *Mater. Chem. Phys.*, 2010, **124**, 694–698.
3 T. T. Tseng and W. J. Tseng, *Ceram. Int.*, 2009, **35**, 2837–2844.
4 S. W. Kuo, Y. C. Chung, K. U. Jeogn and F. C. Chang, *J. Phys. Chem. C*, 2008, **112**, 16470–16477.
5 J. Gong, L. Luo, S. H. Yu, H. Qian and L. Fei, *J. Mater. Chem.*, 2006, **16**, 101–105.
6 Y. C. Lin, C. H. Chen, L. Y. Chen, S. C. Hsu and S. Qia, *RSC Adv.*, 2014, **4**, 45419–45424.
7 K. Amikura, T. Kimura, M. Hamada, N. Yokoyama, J. Miyazaki and Y. Yamada, *Appl. Surf. Sci.*, 2008, **254**, 6976–6982.
8 Z. Paszti, Z. E. Horvath, G. Peto, A. Karacs and L. Guczi, *Appl. Surf. Sci.*, 1997, **109**, 67–73.
9 V. Amendola and M. Meneghetti, *J. Mater. Chem.*, 2007, **17**, 4705–4710.
10 F. Lin, J. Yang, S. H. Lu, K. Y. Niu, Y. Liu, J. Sun and X. W. Du, *J. Mater. Chem.*, 2010, **20**, 1103–1106.
11 X. Zheng, L. Zhu, X. Wang, A. Yan and Y. Xie, *J. Cryst. Growth*, 2004, **260**, 255–262.
12 Z. Wang, Z. Zhao and J. Qiu, *J. Phys. Chem. Solids*, 2008, **69**, 1296–1300.
13 W. M. Cheng, C. C. Wang and C. Y. Chen, *J. Colloid Interface Sci.*, 2010, **348**, 49–56.
14 L. Tang, B. Zhou, J. Zhao, X. Lv, F. Sun and Z. Wang, *Colloids Surf., A*, 2009, **332**, 43–49.
15 L. Wu, Y. Wu, H. Wei, Y. Shi and C. Hu, *Mater. Lett.*, 2004, **58**, 2700–2703.
16 J. Zhao, Z. G. Jin, T. Li and X. X. Liu, *J. Eur. Ceram. Soc.*, 2006, **26**, 2769–2775.
17 Q. R. Hu, S. L. Wang, Y. Zhang and W. H. Tang, *J. Alloys Compd.*, 2010, **491**, 707–711.
18 Y. Zhao, Y. Zhang, Y. Li, Z. He and Z. Yan, *RSC Adv.*, 2012, **2**, 11544–11551.
19 D. T. Nguyen, D. J. Kim, M. G. So and K. S. Kim, *Adv. Powder Technol.*, 2010, **21**, 111–118.
20 Y. Mikhlin, A. Karacharov, M. Likhatski, T. Podlipskaya, Y. Zubavichus, A. Veligzhanin and V. Zaikovski, *J. Colloid Interface Sci.*, 2011, **362**, 330–336.
21 J. Zou, J. Jiang, L. Huang, H. Jiang and K. Huang, *Solid State Sci.*, 2011, **13**, 1261–1267.
22 J. Lu, Z. Ye, J. Huang, L. Wang and B. Zhao, *Appl. Surf. Sci.*, 2003, **207**, 295–299.
23 F. H. Lu, M. M. Mohamed, T. F. Liu, F. C. Chang, C. G. Chao and S. W. Kuo, *J. Mater. Chem. C*, 2014, **2**, 6111–6118.
24 F. Bayansal, H. A. Çetinkara, S. Kahraman, H. M. Çakmak and H. S. Guder, *Ceram. Interfaces*, 2012, **38**, 1859–1866.
25 T. A. Chen, X. Wu and R. D. Rieke, *J. Am. Chem. Soc.*, 1995, **117**, 233–244.
26 P. T. Wu, H. Xin, F. S. Kim, G. Ren and S. A. Jenekhe, *Macromolecules*, 2009, **42**, 8817–8826.
27 M. A. Ibrahim, B. G. Lee, N. G. Park, J. R. Pugh, D. D. Eberl and A. J. Frank, *Synth. Met.*, 1999, **105**, 35–42.
28 Y. Wang, X. Li, N. Wang, X. Quan and Y. Chen, *Sep. Purif. Technol.*, 2008, **62**, 727–732.
29 C. C. Chen, P. Liu and C. H. Lu, *Chem. Eng. J.*, 2008, **144**, 509–513.
30 S. Jayaraman, P. S. Kumar, D. Mangalaraj, D. Rajarathnam, S. Ramakrishna and M. P. Srinivasan, *RSC Adv.*, 2014, **4**, 11288–11294.
31 S. Bai, K. Zhang, J. Sun, D. Zhang, R. Luo, D. Li and C. Liu, *Sens. Actuators, B*, 2014, **197**, 142–148.
32 L. Zhai and R. D. McCullough, *J. Mater. Chem.*, 2004, **14**, 141–143.
33 E. Katsia, N. Huby, G. Tallarida, B. Kutrzeba-Kotowska, M. Perego, S. Ferrari, F. C. Krebs, E. Guziewicz, M. Godlewski, V. Osinniy and G. Luka, *Appl. Phys. Lett.*, 2009, **94**, 143501.
34 K. Noori and F. Giustino, *Adv. Funct. Mater.*, 2012, **22**, 5089–5095.

 This journal is © The Royal Society of Chemistry 2014